Self-assembly-Induced Highly Efficient Electrochemiluminescence of Copper Nanocluster

Zhenqiang Ning[a], Qian Sun[a], Erli Yang[a], Fei Yin[a], Mengyuan Chen[a], Guoqiu Wu[abc], Yuanjian Zhang[a] and Yanfei Shen[abc]*

[a] *Medical School, School of Chemistry and Chemical Engineering, Southeast University, Nanjing 210009, China.*

[b] *Center of Clinical Laboratory Medicine, Zhongda Hospital, Southeast University, Nanjing 210009, China.*

[c] *Jiangsu Provincial Key Laboratory of Critical Care Medicine, Southeast University, Nanjing 210009, China.*

Email: Yanfei.Shen@seu.edu.cn

Abstract

Metal nanocluster has been recently developed as a promising electrochemiluminescence (ECL) emitters due to its unique electronic structure and distinctive optical and electrochemistry properties. However, the low ECL efficiency and high cost are still the serious challenges for metal nanocluster-based ECL emitter. Herein, the self-assembly of 4,6-dimethyl-2-mercaptopyrimidine (DMPM) stabilized copper CuNCs (DMPM-CuNCs) into nanosheets was described in detail for the first time, which significantly strengthening its photoluminescence efficiency from 4.3% to 39.3% and improving its photostability and oxidation stability. Most importantly, the ECL efficiency of self-assembled DMPM-CuNCs (DMPM-CuNCs) was markedly enhanced to 39%, reaching a relative high level of reported metal nanocluster-based ECL emitters. This work propose a simple and effective way to improving inherent ECL performance of CuNCs, providing a new guidance for further development of low-cost and high efficiency ECL emitters.

Keywords:

Copper nanocluster, Self-assembly, Electrochemiluminescence, Cuprophilic interactions

1. Introduction

Electrochemiluminescence (ECL), the electrochemical redox reaction-induced light emission of specific emitters, has inspired extensive research enthusiasm worldwide for decades.[1] Relying on its advantages of low background, high sensitivity, and simple operation, ECL has becoming a powerful technique in the biosensing, imaging and other field.[2] For better applied performance, various ECL emitters have been recently developed, including traditional inorganic, organic complexes, and emerging nanomaterials.[3] These emitters have been preliminarily applied to relevant area but still face big challenges in terms of ECL efficiency, stability, cost, synthetic route, and so on. Hence, the topic about how to developing efficient, low-cost and easier to operate ECL emitters became the focus of interest in ECL research communities.

Metal nanoclusters, which consists of several to a few hundred metal atoms (such as Au, Ag, Cu, etc.) and possess unique electronic structure and distinctive optical and electrochemistry properties,[4] have been considered the ideal ECL emitters for its advantages of multicolor emission, excellent biocompatibility and stability.[3c, 5] However, most of the existing metal nanoclusters-based ECL emitters showed relatively low ECL efficiency, which limited its further application. Recently, a series of strategies have been explored For improving the ECL efficiency of metal nanoclusters, such as regulating charge states and core sizes,[6] covalently linking metal

nanocluster to coreactant,[7] Ag atoms doping,[8] pre-oxidation treatment,[5b] utilizing host-guest recognition,[9] integrating aggregation-induced emission (AIE) and electrocatalytic effects.[10] Although the metal nanocluster with high ECL efficiency had been explored based on those strategies they are nearly all noble metal nanocluster (mainly AuNCs), which leads to the high cost for subsequent application. Copper nanocluster (CuNCs), which possess significant cost advantage over other metal nanocluster, is the perfect candidate for developing novel ECL emitters. However, most existing CuNCs-based ECL emitter still suffer from low efficiency, complex synthetic route and poor stability.[11] Therefore, developing an effective strategy to improve inherent ECL performance of CuNCs is urgently needed.

The pioneer research have demonstrated the self-assembly behavior, a spontaneous organization process of individual components into regular nanostructure, could effectively reinforcing the ability of metal nanocluster in photoluminescence, and catalysis.[12] Although self-assembly induced photoluminescence enhancement of CuNCs were recently reported,[12c, 12e, 13] the relationship between self-assembly and ECL of CuNCs has never been described. Herein, we describe the solvent-induced self-assembly of 4,6-dimethyl-2-mercaptopyrimidine (DMPM) stabilized CuNCs (DMPM-CuNCs) into nanosheets (SA-DMPM-CuNCs) in aqueous solution, which possess great advantages of easy preparation, timesaving to previous work.

Moreover, the photoluminescence absolute quantum yield of SA-DMPM-CuNCs was heightened from 4.3% to 39.3% by self-assembly, and its photostability and oxidation stability were significantly improved. More importantly, the assemlied SA-DMPM-CuNCs shows excellent ECL performance with ECL efficiency as high as 39%.

2. Experimental section

2.1 Materials and Reagents

Tris(2,2'-bipyridyl)dichlororuthenium(II) hexahydrate ($Ru(bpy)_3Cl_2 \cdot 6H2O$), Triethylamine (TEA) and Tripropylamine (TPA) were purchased from Sigma-Aldrich Chemical Co. (St. Louis, MO, U.S.A.). 4,6-Dimethyl-2-mercaptopyrimidine (DMPM) and $Cu(NO_3)_2$ were purchased from Macklin Biochemical Co., Ltd. (Shanghai, China) , N,N-Diethylethylenediamine (DEEA) and 2-(Dibutylamino)ethanol (DBAE) were purchased from Aladdin Biochemical Technology Co., Ltd. (Shanghai, China).

2.2 Apparatus

The transmission electron microscopy (TEM) characterization was performed on the Talos F200X transmission electron microscope (Thermo Scientific, USA). The scanning electron microscope (SEM) characterization was carried out with the Gemini 300 field emission scanning electron microscope (Zeiss, Germany). The atomic force microscope (AFM) characterization was carried out with Dimension Icon AFM systems (Bruker, Germany). The X-ray photoelectron spectroscopy (XPS) characterization was performed by K-Alpha automated XPS system (Thermo Scientific, USA). The Fourier transform infrared spectroscopy (FTIR) spectrum was collected by Nicolet iS20 FT-IR Spectrometer (Thermo Scientific, USA). The photoluminescence (PL) spectra were

analyzed with the Fluoromax-4 fluorescence spectrometer (Horiba, Japan). The ultraviolet-visible (UV-vis) absorption spectra were recorded using a Cary100 UV-vis spectrophotometer (Agilent, USA). The electrochemical measurements were performed with a CHI660E electrochemical workstation (CHI, China). The electrochemiluminescence (ECL) measurements were carried out with an MPI-EII ECL analyzer system (Xi'an Remex, China). All the electrochemical experiments were performed with a conventional three-electrode system containing a platinum wire as a counter electrode, an Ag/AgCl as a reference electrode, and a glassy carbon electrode (GCE, d=3 mm) as a working electrode.

2.3 Preparation of DMPM-CuNCs

5 mL of 25 mM $Cu(NO_3)_2$ ethanol solution was mixed with 5 mL of 40 mM DMPM ethanol solution under magnetic stirring at room temperature. Ten minutes later, the grey-brown DMPM-CuNCs solution was obtained. For purification, the DMPM-CuNCs raw products were first collected by centrifugation, and then washed by ethanol solution for three times. The resultant precipitates were dispersed in 10 mL dimethyl sulfoxide (DMSO) to form a faint yellow DMPM-CuNCs solution.

2.4 Preparation of SA-DMPM-CuNCs

5 mL of 25 mM $Cu(NO_3)_2$ ethanol solution was mixed with 5 mL of 40 mM DMPM ethanol solution under magnetic stirring at room temperature. Ten minutes later, the grey-brown DMPM-CuNCs solution was obtained. For purification, the DMPM-CuNCs raw products were first collected by centrifugation, and then washed by ethanol solution for three times. The resultant precipitates were re-dispersed by water with

magnetic stirring or ultrasonic treatment for more than 1 h, DMPM-CuNCs were spontaneously assembled into nanosheets during this process.

2.5 Gram-scale synthesis of SA-DMPM-CuNCs

500 mL of 5 mM $Cu(NO_3)_2$ aqueous solution was mixed with 500 mL of 8 mM DMPM aqueous solution under magnetic stirring at room temperature for more than 1 h. The resulted SA-DMPM-CuNCs nanosheets was collected via centrifugation and washed by water for three time.

2.5 Determination of the relative ECL efficiency

The relative ECL efficiency (Φ_{ECL}) of SA-DMPM-CuNCs were measured according to the previously reported method [5b, 14]. By using $Ru(bpy)_3^{2+}$ as a reference standard, Φ_{ECL} was calculated through the following formula:

$$\Phi_{ECL}=\Phi_{ECL}^{0}\,(IQ_f^{0}/I^{0}Q_f)$$

Where Φ_{ECL}^{0} is the ECL efficiency of 1 mM $Ru(bpy)_3^{2+}$ in 0.1 M TBAP/acetonitrile solution via annihilation pathway, which was measured as 5%[15]; I^0 and I are the ECL intensities of $Ru(bpy)_3^{2+}$ (1 mM) and SA-DMPM-CuNCs modified GCE, respectively; Q_f^0 and Q_f are the corresponding faradaic charge passed during the ECL measurement for $Ru(bpy)_3^{2+}$ and SA-DMPM-CuNCs, respectively.

For I^0 and Q_f^0 determination of reference standard (1 mM $Ru(bpy)_3^{2+}$), the acetonitrile solution containing 0.1 M TBAP was served as supporting electrolyte, and the ECL intensity and current response of working electrode were recorded under a cyclic double potential scanning from -1.4 V to +1.3 V. While for I and Q_f measurement, the cyclic double potential scanning of SA-DMPM-CuNCs modified working electrode was

carried out in 0.01 M PBS (pH=7.4) solution containing 75 mM TEA, and the ECL intensity and current response were recorded.

3. Results and Discussion

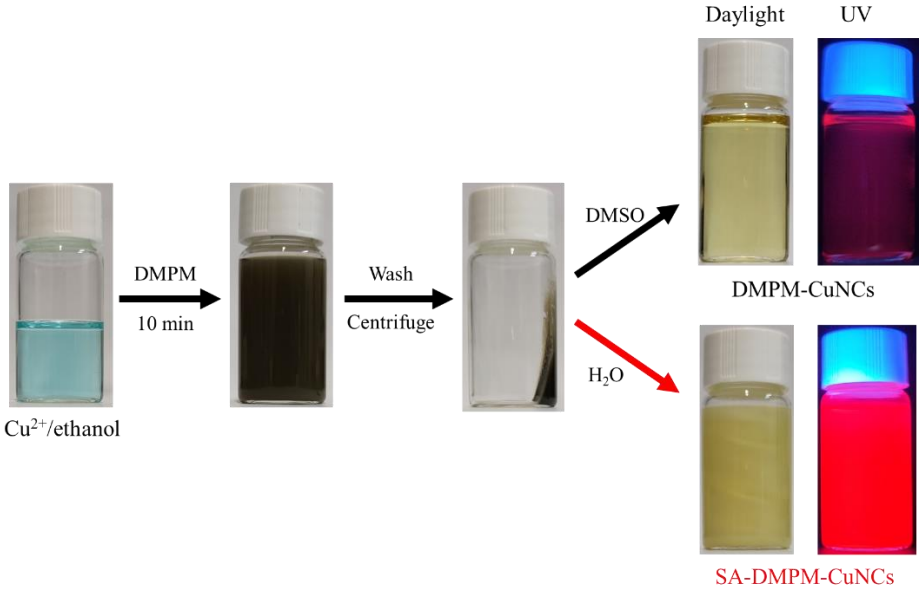

Figure 1. The preparation process of DMPM-CuNCs and SA-DMPM-CuNCs.

Herein, we introduce a facile one-pot strategy for synthesizing CuNCs by using 4, 6-dimethyl-2-mercaptopyrimidine (DMPM) as the capping ligand and reductant in ethanol solution. As shown in Figure 1, the brownish-gray precipitates were collected by centrifuging the reaction product of Cu^{2+} and DMPM. The resulted DMPM-CuNCs precipitates can be re-dispersed in DMSO to forming a transparent and faint yellow solution, which exhibiting weak photoluminescence under UV radiation. However, when suspending in water, DMPM-CuNCs precipitates was transformed into yellow suspension, which emitting significantly enhanced red photoluminescence under UV radiation, namely SA-DMPM-CuNCs (Figure 1). TEM observation indicated that

DMPM-CuNCs are monodispersed nanoparticles with the average diameter of 1.40 nm (Figure 2a), and SA-DMPM-CuNCs appear as regular nanosheets which consisted of monodispersed clusters with the average diameter of 1.21 nm (Figure 2b and 2c). In addition, EDS-mapping result confirms that Cu and S elements were uniformly distributed over the entire SA-DMPM-CuNCs nanosheets (Figure 2d-f). SEM and AFM image reveals that DMPM-CuNCs were assembled into numerous square nanosheets with the side length about 2-5 μm, thickness about 10 nm (Figure 2g-i). The above results clearly confirmed the self-assembly behavior of SA-DMPM-CuNCs in water. It is worth noting that the self-assembly strategy of SA-DMPM-CuNCs proposed in present work, which requires no special additive and takes less than an hour (Figure S1), is more convenience and efficient than the previous work.[12d-f]

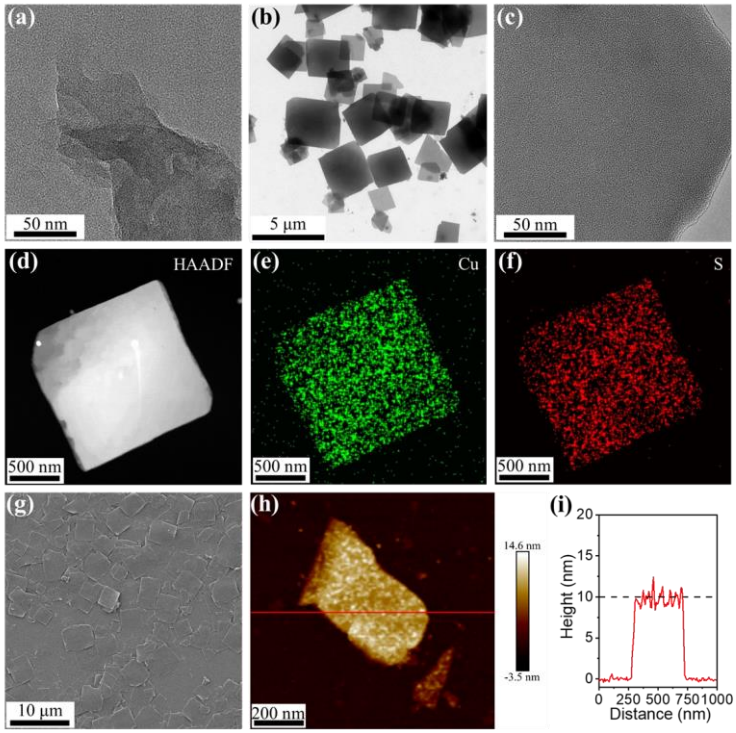

Figure 2. TEM characterization of (a) DMPM-CuNCs and (b, c) SA-DMPM-CuNCs nanosheets at 500 nm and 50 nm scale, respectively. (d-f) EDS-mapping images of SA-DMPM-CuNCs nanosheets. (g) SEM, (h) AFM characterization and (i) corresponding height profile of SA-DMPM-CuNCs nanosheets.

To explore compositional information of the CuNCs, FTIR and XPS analysis of DMPM-CuNCs and SA-DMPM-CuNCs were performed. As shown in Figure 3a, the characteristic peaks at 2865, 1741, 1215, 1187 and 471 cm^{-1} which corresponds to the thiol group-related vibration of DMPM molecules,[16] were disappeared in the FTIR spectra of DMPM-CuNCs and SA-DMPM-CuNCs, confirming the successful synthesis of thiolate-stabilized CuNCs. In addition, SA-DMPM-CuNCs retained all the FTIR features of DMPM-CuNCs, indicating that there is no appearance or disappearance of chemical bond during self-assembly process. XPS survey spectrum of the CuNCs demonstrated the existence of C, N, S and Cu elements in DMPM-CuNCs and SA-DMPM-CuNCs (Figure S2). The Cu2p high-resolution spectra in Figure 2b and 2d both showed two intense peaks around 932.3 eV and 952.2 eV assigned to the $Cu2p_{3/2}$ and $Cu2p_{1/2}$ signals of Cu(0) or Cu(I) species,[11b] and no satellite peak of Cu(II) electrons around 942.0 eV was observed, evidencing that Cu(II) was adequately reduced by DMPM molecular during the synthesis of DMPM-CuNCs and SA-DMPM-CuNCs.[17] Besides, the S2p spectra indicated the peaks around 162.2 eV and 163.5eV, which were assigned to $S2p_{3/2}$ and $S2p_{1/2}$ electrons. Due to the binding energy of $S2p_{3/2}$ around 162 eV is belong to the sulfur bonded to metal atoms,[18] Cu-S bonding formation in DMPM-CuNCs and SA-DMPM-CuNCs were confirmed. The above results verified the typical thiolate-stabilized CuNCs components of DMPM-CuNCs and SA-DMPM-CuNCs.

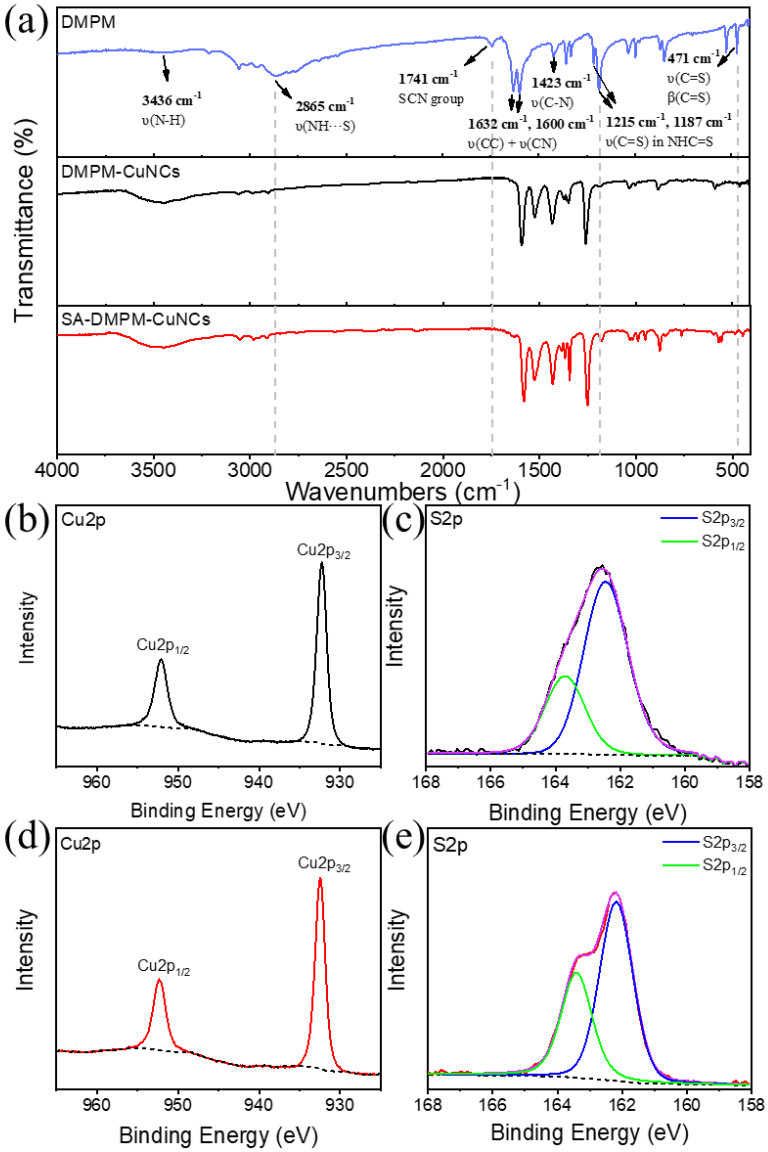

Figure 3. (a) FTIR spectrum of DMPM ligand, DMPM-CuNCs and DMPM-CuNCs. (b) XPS Cu2p and (c) S2p high-resolution spectrum of DMPM-CuNCs. (d) XPS Cu2p and (e) S2p high-resolution spectrum of SA-DMPM-CuNCs.

For unraveling the self-assembly mechanism, the solvents with different polarity were employed to dispersing DMPM-CuNCs precipitates. As shown in Figure 4a, DMPM-CuNCs were soluble in DMSO and DMF and exhibited weak photoluminescence emission, and its self-assembly process was activated just in water, indicating that solvent is the critical factor for the self-assembly behavior of SA-

DMPM-CuNCs. To get more information about the compositional change during the self-assembly reaction, UV-vis absorption and FL spectra of these two CuNCs were detected. As shown in Figure S3, original DMPM-CuNCs indicated three characteristic absorption peaks at 257, 274 and 298 nm, and a photoluminescence emission peak around 700 nm; however, the assembled SA-DMPM-CuNCs exhibited one absorption peaks at 324 nm, and a photoluminescence emission peak around 678 nm. The difference in UV-Vis absorption and FL spectra of DMPM-CuNCs and SA-DMPM-CuNCs suggested the structural or compositional changes of CuNCs during self-assembly process. In addition, the Cu LMM Auger spectra shows the Cu(I)/Cu(0) molar ratio of DMPM-CuNCs and SA-DMPM-CuNCs are 2.02 and 2.22 (Figure 4b and 4c), i.e. Cu(I) species was increased after SA-DMPM-CuNCs self-assembly. Considering that FTIR confirmed no appearance or disappearance of chemical bond during self-assembly process, the Cu(I) content variation might be caused by surface-motif reconstruction of DMPM-CuNCs.[12d] It is interesting to note that the cuprophilic Cu(I)···Cu(I) interaction have proven to play a key role in the self-assembly of CuNCs, which might be limited by low Cu(I) content or long intercluster Cu(I)···Cu(I) distance.[12d-f, 19] Therefore, in present work, the higher Cu(I) content laid the physical foundation for the self-assembly of SA-DMPM-CuNCs. Furthermore, the self-assembly mechanism of SA-DMPM-CuNCs could be deduced as follow: Firstly, DMPM-CuNCs could be destabilized when dispersing in water, and the surface-motif reconstruction process was activated, which lead to the Cu(I) content increased; Secondly, the hydrophobic effect could promoted CuNCs with high Cu(I) content close

to each other, inducing the strong intercluster cuprophilic interaction of DMPM-CuNCs; Finally, the π-π interaction of DMPM ligands might assisted DMPM-CuNCs assembled to regular multi-layer nanosheets. On the basis of such hypothesis, we were trying to directly synthesizing SA-DMPM-CuNCs in aqueous phase. Surprisingly, Gram-scale synthesis of SA-DMPM-CuNCs was readily achieved by this way (Figure S4). It is worth mentioning that this innovative strategy to synthesizing self-assembled metal nanoclusters first proposed in present work is far easier and more efficient than the existing methods.[12a, 12d, 20]

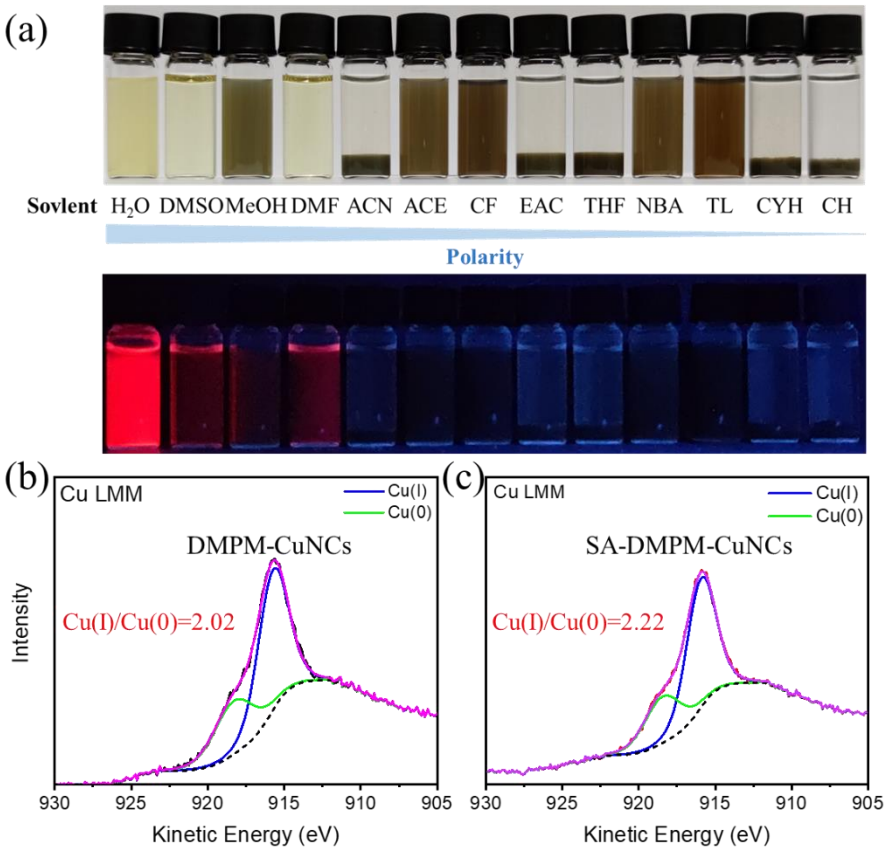

Figure 4. (a) Photos of DMPM-CuNCs precipitates dispersed in the solvents with different polarity under visible (top row) and UV (bottom row) light. XPS Cu LMM Auger spectra of (b) DMPM-CuNCs and (c) SA-DMPM-CuNCs.

Interestingly, the self-assembly behavior endows SA-DMPM-CuNCs with

significantly improved photoluminescence performances. As shown in Figure 5a, the photoluminescence emission intensity of SA-DMPM-CuNCs was greatly strengthened by 15.1 fold than the original DMPM-CuNCs. In addition, the absolute quantum yield of SA-DMPM-CuNCs was measured up to 39.3%, which is remarkably higher than the unassembled DMPM-CuNCs (4.3%) and most of the reported CuNCs.[12e, 12f, 17, 19a, 21] Furthermore, the average photoluminescence lifetime of SA-DMPM-CuNCs was prolonged from 4.09 μs to 11.50 μs after self-assembly (Figure 5b). The μs-level lifetimes and super large stokes-shift (>330 nm, Figure S3) supported the PL emission of DMPM-CuNCs and SA-DMPM-CuNCs were mainly phosphorescence, originating from ligand-to-metal charge transfer (LMCT) on the basis of metal-centered triplet state, which was commonly observed in the thiolate-stabilized metal nanoclusters.[17, 22] The self-assembly induced emission enhancement was possibly ascribed to the dense packing of DMPM-CuNCs in assembled nanosheets, which effectively restricts the intramolecular vibration and rotation of Cu(I)-DMPM motifs, leading to the reduction of non-radiative relaxation and emission enhancement.[12c, 23] In addition, the blue-shift emission of SA-DMPM-CuNCs (Figure S3) has been previously attributed to the enhanced intercluster cuprophilic interaction.[17, 21, 24] Apart from emission intensity, the instability of CuNCs toward airs (e.g. O_2) or light radiation (e.g. UV) are still the serious challenges in their application.[25] In present work, the self-assembled CuNCs protected by the compact surface ligand showed excellent stability in UV radiation and oxidation conditions (Figure 5b and 5c), which is advantageous for subsequent research and application.

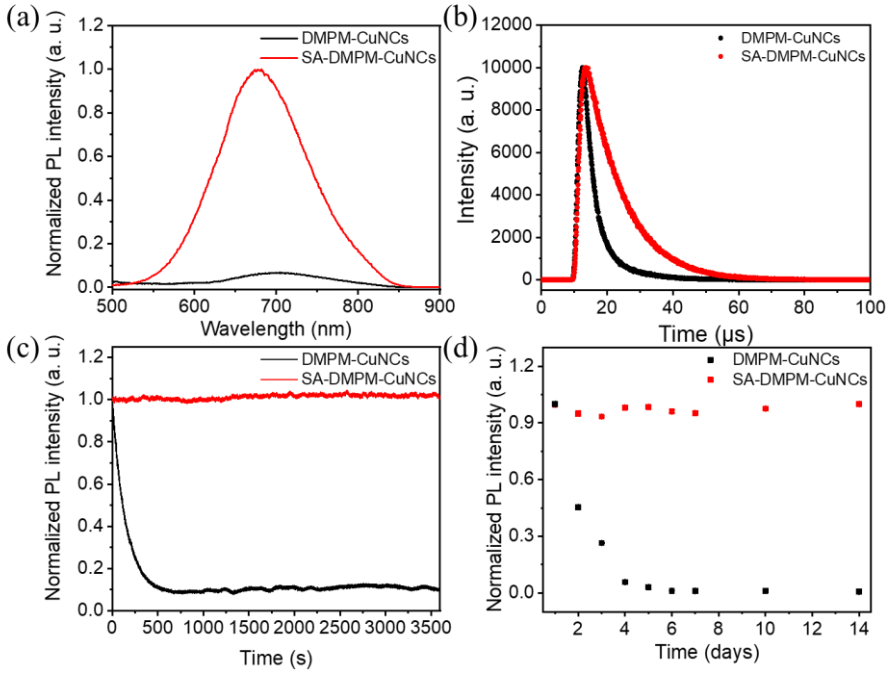

Figure 5. (a) Photoluminescence emission spectra of DMPM-CuNCs (black) and SA-DMPM-CuNCs (red). (b) Photoluminescence decay profiles of DMPM-CuNCs (black) and SA-DMPM-CuNCs (red). (c) Photostability of DMPM-CuNCs (black) and SA-DMPM-CuNCs (red) under continuous 3500 s radiation at maximum excitation wavelength. (d) Oxidative stability of DMPM-CuNCs (black) and SA-DMPM-CuNCs (red) stored at room temperature under ambient conditions for 14 days.

Next, annihilation ECL property of both the DMPM-CuNCs and SA-DMPM-CuNCs was studied by CV scanning between ±1.4 V. As shown in Figure S5a, differing from absent ECL signal of DMPM-CuNCs, the evident annihilation ECL was detected in SA-DMPM-CuNCs. To investigate the annihilation ECL process, the electrochemistry behavior of SA-DMPM-CuNCs was tested first. As shown in Figure S5b, three reduction peaks at -0.28 V (R1), -0.59 V (R2) and -1.13 V (R3), and three oxidation peaks at 0.19 V (O1), 0.5 V (O2) and 1.2 V (O3) were found during the cathodic and anodic DPV scanning of SA-DMPM-CuNCs. Then, the self-annihilation reactions between the reductive and oxidative states of SA-DMPM-CuNCs were monitored by stepping pulse approach. The transient ECL of SA-DMPM-CuNCs was

observed until the initial potential down to -1.13 V (Figure 6c), when stepping potential from each reductive potentials (-0.28 V, -0.59 V and -1.13 V) to 1.2 V, respectively. Besides, no transient ECL was detected by stepping potential from -1.13 V to 0.19 V and 0.5 V. These evidence showed the ECL of SA-DMPM-CuNCs in aqueous solution was generated based on the self-annihilation reaction between reduced SA-DMPM-CuNCs^{3-} and oxidized SA-DMPM-CuNCs^{3+} species, which produced excited state SA-DMPM-CuNCs^{2+*} for ECL emission.

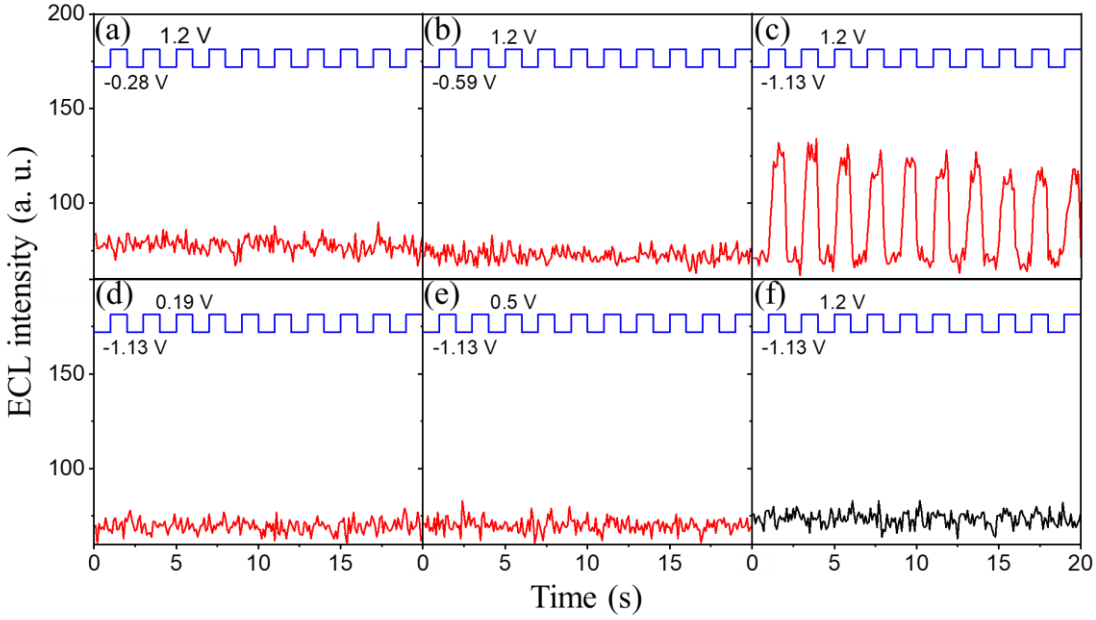

Figure 6. Transient ECL of (a-e) GCE/SA-DMPM-CuNCs and (f) bare GCE in 0.1 M PBS by stepping the potential from (a) -0.28 to 1.2 V, (b) -0.59 to 1.2 V, (c) -1.13 to 1.2 V, (d) -1.13 to 0.19 V, (e) -1.13 to 0.5 V and (f) -1.13 to 1.2 V every 1 s. The blue curves indicate the applied potential steps.

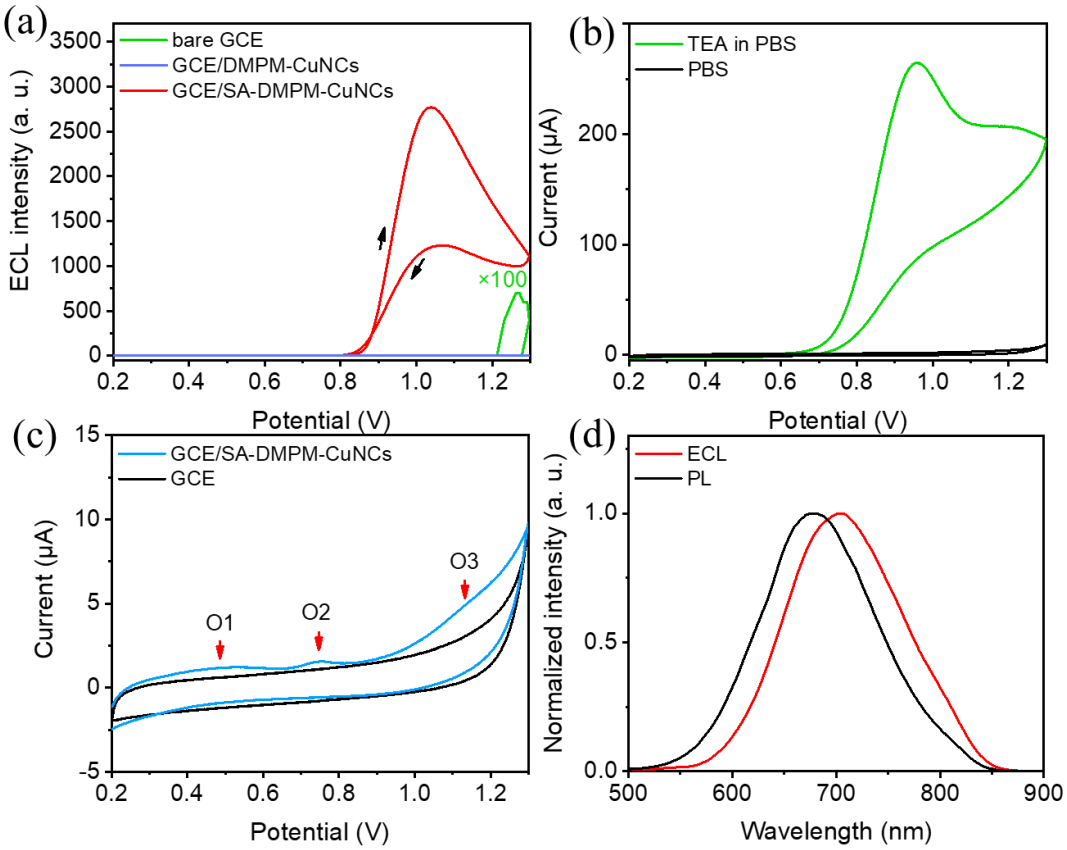

Figure 7. (a) ECL curves of bare GCE (green), GCE/SA-DMPM-CuNCs (red) in 0.01 M PBS containing 75 mM TEA, and GCE/DMPM-CuNCs (blue) in CAN containing 0.1 M TBAP and 75 mM TEA. (b) CV curves of bare GCE in 0.01 M PBS with (green) and without (black) 75 mM TEA. (c) CV curves of bare GCE (black) and GCE/SA-DMPM-CuNCs (blue) in 0.01 M PBS. (d) ECL and PL spectra of SA-DMPM-CuNCs, ECL spectra of GCE/SA-DMPM-CuNCs was measured in 0.01 M PBS with 75 mM TEA.

Then, the ECL behavior of DMPM-CuNCs and SA-DMPM-CuNCs at coreactant pathway were further investigated under CV scanning. As shown in Figure 7a, no ECL signal was observed from GCE/DMPM-CuNCs in PBS electrolyte with the existing of TEA coreactant. Surprisingly, the GCE/SA-DMPM-CuNCs showed intense ECL emission, which is order of magnitudes higher than the background signal of TEA (Figure 7a), verifying the self-assembly induced ECL property of SA-DMPM-CuNCs. To gain insight into the coreactant ECL mechanism of SA-DMPM-CuNCs, CV curves

of TEA and SA-DMPM-CuNCs were recorded, respectively. As shown in Figure 7b and 7c, TEA showed a board oxidation process with onset potential at 0.64 V, while SA-DMPM-CuNCs exhibited three oxidation processes with onset potential at approximately 0.35 V, 0.66 V and 0.86 V. It is worth noting that the ECL emission of SA-DMPM-CuNCs was generated until the potential scanning to 0.86 V, which is highly consistent with the onset potential of 3st oxidation, indicating the 3st oxidative product, i. e. SA-DMPM-CuNCs^{3+} could reacted with coreactant radical to form the exited state SA-DMPM-CuNCs^{2+*} for light emission. Notably, the ECL spectrum of SA-DMPM-CuNCs a distinct peak around 700 nm, which is slightly red-shifted to the PL emission peak at 678 nm (Figure 7d). The red-shift ECL emission of SA-DMPM-CuNCs could be attributed to self-absorption and inner-filter effects in ECL reaction.[6, 26] Based on the above data, the possible ECL mechanism could be inferred as follow:

$$TEA + e^- \rightarrow TEA^{\bullet+} \rightarrow TEA^{\bullet} + H^+ \quad (1)$$

$$\text{SA-DMPM-CuNCs} - e^- \rightarrow \text{SA-DMPM-CuNCs}^{1+} \quad (2)$$

$$\text{SA-DMPM-CuNCs}^{1+} - e^- \rightarrow \text{SA-DMPM-CuNCs}^{2+} \quad (3)$$

$$\text{SA-DMPM-CuNCs}^{2+} - e^- \rightarrow \text{SA-DMPM-CuNCs}^{3+} \quad (4)$$

$$TEA^{\bullet} + \text{SA-DMPM-CuNCs}^{3+} \rightarrow \text{SA-DMPM-CuNCs}^{2+*} \quad (5)$$

$$\text{SA-DMPM-CuNCs}^{2+*} \rightarrow \text{SA-DMPM-CuNCs}^{2+} + h\nu \quad (6)$$

Under the optimum conditions (Figure S6), the ECL performance of SA-DMPM-CuNCs was examined by using TEA as coreactant. Benefiting from the sheet structure, SA-DMPM-CuNCs could directly modified on the work electrode and showed excellent ECL signal stability (Figure S7), which is friendly for subsequent ECL application. More importantly, the ECL efficiency (Φ_{ECL}) of SA-DMPM-CuNCs was

determined as 39%, which was much better than the previously reported various ECL emitter, including metal nanoclusters (Table 1). In this work, the ECL performance of SA-DMPM-CuNCs was markedly improved after experiencing a simple self-assembly reaction, which was ascribed to the suppressed intramolecular rotation and vibration of ligand DMPM on the compactly packed CuNCs, greatly restraining the nonradiative relaxation.[10] Due to its advantages of easy preparation, low cost and excellent ECL performance, SA-DMPM-CuNCs proposed in present work exhibiting promising future for ECL-related applications.

Table 1. ECL efficiency comparation of previously reported ECL emitters.

ECL emitter	**Coreactant**		**Φ_{ECL} (%)**	**Reference**
	Tpye	**Concentration**		
$[Ru(bpy)_2PIC]^{2+}$ loaded polyaniline	TPA	50 mM	1	[27]
$[Ru(bpy)_2(PVP)_{10}]^{2+}$	TPA	100 mM	9.2	[14b]
Cd–In–S nanoclusters	TPA	20 mM	2.1	[28]
	$K_2S_2O_8$	20 mM	0.13	[28]
BN QDs	$K_2S_2O_8$	100 mM	1.04	[29]
S-BN QDs^L	$K_2S_2O_8$	100 mM	2.69	[29]
S-BN QDs^T	$K_2S_2O_8$	100 mM	3.78	[29]
Met-AuNCs	$K_2S_2O_8$	100 mM	2.23	[10]
BSA-AuNCs	$K_2S_2O_8$	100 mM	0.33	[10]

NAC-AuNCs	$K_2S_2O_8$	100 mM	4.11	[30]
GSH-AuNCs	TEA	300 mM	0.42	[5b]
BSA-AuNCs	TEA	300 mM	9.8	[5b]
Ox-Met-AuNCs	TEA	300 mM	66	[5b]
ATT-AuNCs	TEA	140 mM	78	[10]
MPP-CuNCs*	TPA	5 mM	0.74	[31]
DMPM-CuNCs	TEA	75 mM	No signal	This work
SA-DMPM-CuNCs	TEA	75 mM	39	This work

4. Conclusions

In conclusion, the fast and convenient self-assembly of DMPM stabilized CuNCs was achieved through solvent-induced approach in the aqueous solution. The DMPM-CuNCs was self-assembled into compact and ordered nanosheets relying on cuprophilic interactions, π-π interaction, and hydrophobic effect etc., which effectively restricts the intramolecular vibration and rotation of Cu(I)-DMPM motifs, leading to the reduction of non-radiative relaxation and PL emission enhancement. In addition, the self-assembly behavior of SA-DMPM-CuNCs was demonstrated an effective way to overcame the weakness of traditional CuNCs in photostability and oxidation stability. More importantly, the self-assembled SA-DMPM-CuNCs showed excellent ECL performance in aqueous solutions with Φ_{ECL} as high as 39%, which is significantly higher than the reported CuNCs-based ECL emitters. This research proposed a versatile strategy to improving inherent PL and ECL properties of CuNCs, which would

promotes the mechanistic understanding on self-assembly behavior of CuNCs, and provides a new avenue for preparing low-cost and efficient CuNCs-based PL and ECL emitters in biosensing or imaging application.

Acknowledgements

This work is supported by the National Natural Science Foundation of China (22074015 and 21775018).

References

[1] a) R. Luo, H. Lv, Q. Liao, N. Wang, J. Yang, Y. Li, K. Xi, X. Wu, H. Ju, J. Lei, *Nat. Commun.* **2021**, *12*, 6808; b) X. Ma, W. Gao, F. Du, F. Yuan, J. Yu, Y. Guan, N. Sojic, G. Xu, *Accounts Chem. Res.* **2021**, *54*, 2936-2945; c) Z. Ning, M. Chen, G. Wu, Y. Zhang, Y. Shen, *Biosens. Bioelectron.* **2021**, *191*, 113462.

[2] a) K. G. Cho, J. I. Lee, S. Lee, K. Hong, M. S. Kang, K. H. Lee, *Adv. Funct. Mater.* **2020**, *30*, 1907936; b) Y. Liu, H. Zhang, B. Li, J. Liu, D. Jiang, B. Liu, N. Sojic, *J. Am. Chem. Soc.* **2021**, *143*, 17910-17914; c) J. Dong, Y. Lu, Y. Xu, F. Chen, J. Yang, Y. Chen, J. Feng, *Nature* **2021**, *596*, 244-249; d) J. I. Lee, H. Choi, S. H. Kong, S. Park, D. Park, J. S. Kim, S. H. Kwon, J. Kim, S. H. Choi, S. G. Lee, D. H. Kim, M. S. Kang, *Adv. Mater.* **2021**, *33*, 2100321.

[3] a) P. Wu, X. Hou, J.-J. Xu, H.-Y. Chen, *Chem. Rev.* **2014**, *114*, 11027-11059; b) A. Abdussalam, G. Xu, *Anal. Bioanal. Chem.* **2021**; c) Z. Liu, W. Qi, G. Xu, *Chem. Soc. Rev.* **2015**, *44*, 3117-3142.

[4] a) R. Jin, G. Li, S. Sharma, Y. Li, X. Du, *Chem. Rev.* **2021**, *121*, 567-648; b) X. Kang, M. Zhu, *Chem. Soc. Rev.* **2019**, *48*, 2422-2457; c) Y. Tao, M. Li, J. Ren, X. Qu, *Chem. Soc. Rev.* **2015**, *44*, 8636-8663; d) X. Kang, Y. Li, M. Zhu, R. Jin, *Chem. Soc. Rev.* **2020**, *49*, 6443-6514.

[5] a) M. Hesari, Z. Ding, *J. Am. Chem. Soc.* **2021**, *143*, 19474-19485; b) H. Peng, Z. Huang, Y. Sheng, X. Zhang, H. Deng, W. Chen, J. Liu, *Angewandte Chemie International Edition* **2019**, *58*, 11691-11694.

[6] M. Hesari, Z. Ding, *Accounts Chem. Res.* **2017**, *50*, 218-230.

[7] T. Wang, D. Wang, J. W. Padelford, J. Jiang, G. Wang, *J. Am. Chem. Soc.* **2016**, *138*, 6380-6383.

[8] S. Chen, H. Ma, J. W. Padelford, W. Qinchen, W. Yu, S. Wang, M. Zhu, G. Wang, *J. Am. Chem. Soc.* **2019**, *141*, 9603-9609.

[9] L. Yang, B. Zhang, L. Fu, K. Fu, G. Zou, *Angew. Chem. Int. Ed.* **2019**, *58*, 6901-6905.

[10] H. Peng, Z. Huang, H. Deng, W. Wu, K. Huang, Z. Li, W. Chen, J. Liu, *Angew. Chem. Int. Ed.* **2020**, *59*, 9982-9985.

[11] a) M.-C. Pan, Y.-M. Lei, Y.-Q. Chai, R. Yuan, Y. Zhuo, *Anal. Chem.* **2020**, *92*, 13581-13587; b) W. Wei, Y. Lu, W. Chen, S. Chen, *J. Am. Chem. Soc.* **2011**, *133*, 2060-2063; c) M. Zhao, A.-Y. Chen, D. Huang, Y. Zhuo, Y.-Q. Chai, R. Yuan, *Anal. Chem.* **2016**, *88*, 11527-11532.

[12] a) Z. Wu, Q. Yao, S. Zang, J. Xie, *ACS Mater. Lett.* **2019**, *1*, 237-248; b) Z. Wu, Y. Li, J. Liu, Z. Lu, H. Zhang, B. Yang, *Angew. Chem. Int. Ed.* **2014**, *53*, 12196-12200; c) X. Ouyang, M. Wang, L. Guo, C. Cui, T. Liu, Y. Ren, Y. Zhao, Z. Ge, X. Guo, G. Xie, J. Li, C. Fan, L. Wang, *Angew. Chem. Int. Ed.* **2020**, *59*, 11836-11844; d) Z. Wu, Y. Du, J. Liu, Q. Yao, T. Chen, Y. Cao, H. Zhang, J. Xie, *Angew. Chem. Int. Ed.* **2019**, *58*, 8139-8144; e) Z. Wu, H. Liu, T. Li, J. Liu, J. Yin, O. F. Mohammed, O. M. Bakr, Y. Liu, B. Yang, H. Zhang, *J. Am. Chem. Soc.* **2017**, *139*, 4318-4321; f) Z. Wu, J. Liu, Y. Gao, H. Liu, T. Li, H. Zou, Z. Wang, K. Zhang, Y. Wang, H. Zhang, B. Yang, *J. Am. Chem. Soc.* **2015**, *137*, 12906-12913.

[13] D. Bera, N. Goswami, *J. Phys. Chem. Lett.* **2021**, *12*, 9033-9046.

[14] a) W. L. Wallace, A. J. Bard, *J. Phys. Chem.* **1979**, *83*, 1350-1357; b) L. Dennany, C. F. Hogan, T. E. Keyes, R. J. Forster, *Anal. Chem.* **2006**, *78*, 1412-1417.

[15] N. E. Tokel-Takvoryan, R. E. Hemingway, A. J. Bard, *J. Am. Chem. Soc.* **1973**, *95*, 6582-6589.

[16] R. Martos-Calvente, V. A. de la Peña O'Shea, J. M. Campos-Martin, J. L. G. Fierro, *J. Phys. Chem. A* **2003**, *107*, 7490-7495.

[17] Z. Wang, B. Chen, A. S. Susha, W. Wang, C. J. Reckmeier, R. Chen, H. Zhong, A. L. Rogach, *Adv. Sci.* **2016**, *3*, 1600182.

[18] a) A. W. Snow, E. E. Foos, M. M. Coble, G. G. Jernigan, M. G. Ancona, *Analyst* **2009**, *134*, 1790-1801; b) T. P. Ang, T. S. A. Wee, W. S. Chin, *J. Phys. Chem. B* **2004**, *108*, 11001-11010.

[19] a) S. Nematulloev, R.-W. Huang, J. Yin, A. Shkurenko, C. Dong, A. Ghosh, B. Alamer, R. Naphade, M. N. Hedhili, P. Maity, M. Eddaoudi, O. F. Mohammed, O. M. Bakr, *Small* **2021**, *17*, 2006839; b) X. Su, J. Liu, *ACS Appl. Mater. Interfaces* **2017**, *9*, 3902-3910.

[20] a) Y. Liu, D. Yao, H. Zhang, *ACS Appl. Mater. Interfaces* **2018**, *10*, 12071-12080; b) Z. Liu, D. Yao, L. Ai, H. Liu, S. Zhang, H. Zhang, *Soft Matter* **2021**, *17*, 4550-4558; c) Z. Wu, Y. Li, J. Liu, Z. Lu, H. Zhang, B. Yang, *Angew. Chem. Int. Ed.* **2014**, *126*, 12392-12396.

[21] Z. Wang, Y. Xiong, S. V. Kershaw, B. Chen, X. Yang, N. Goswami, W.-F. Lai, J. Xie, A. L. Rogach, *Chem. Mat.* **2017**, *29*, 10206-10211.

[22] a) Z. Luo, X. Yuan, Y. Yu, Q. Zhang, D. T. Leong, J. Y. Lee, J. Xie, *J. Am. Chem. Soc.* **2012**, *134*, 16662-16670; b) A. Jana, M. Jash, A. K. Poonia, G. Paramasivam, M. R. Islam, P. Chakraborty, S. Antharjanam, J. Machacek, S. Ghosh, K. N. V. D. Adarsh, T. Base, T. Pradeep, *ACS Nano* **2021**, *15*, 15781-15793.

[23] a) Z. Wu, Q. Yao, O. J. H. Chai, N. Ding, W. Xu, S. Zang, J. Xie, *Angew. Chem. Int. Ed.* **2020**, *59*, 9934-9939; b) H.-H. Deng, X.-Q. Shi, F.-F. Wang, H.-P. Peng, A.-L. Liu, X.-H. Xia, W. Chen, *Chem. Mat.* **2017**, *29*, 1362-1369.

[24] a) Y.-e. Shi, X. Zhuang, L. Cao, S. Gou, Y. Xiong, W.-F. Lai, Z. Wang, A. L. Rogach, *ChemNanoMat* **2019**, *5*, 110-115; b) Q. Benito, X. F. Le Goff, S. Maron, A. Fargues, A. Garcia, C. Martineau, F. Taulelle, S. Kahlal, T. Gacoin, J.-P. Boilot, S. Perruchas, *J. Am. Chem. Soc.* **2014**, *136*, 11311-11320.

[25] a) Y. Song, Y. Li, M. Zhou, X. Liu, H. Li, H. Wang, Y. Shen, M. Zhu, R. Jin, *Sci. Adv.* **2021**, *7*, eabd2091; b) A. Chen, X. Kang, S. Jin, W. Du, S. Wang, M. Zhu, *J. Phys. Chem. Lett.* **2019**, *10*, 6124-6128; c) P. Concepción, M. Boronat, S. García-García, E. Fernández, A. Corma, *ACS Catal.* **2017**, *7*, 3560-3568.

[26] M. Hesari, M. S. Workentin, Z. Ding, *ACS Nano* **2014**, *8*, 8543-8553.

[27] K. M. Molapo, A. Venkatanarayanan, C. M. Dolan, U. Prendergast, P. G. Baker, E. I. Iwuoha, T. E. Keyes, R. J. Forster, *Electrochem. Commun.* **2014**, *48*, 95-98.

[28] F. Wang, J. Lin, T. Zhao, D. Hu, T. Wu, Y. Liu, *J. Am. Chem. Soc.* **2016**, *138*, 7718-7724.

[29] Y. Liu, M. Wang, Y. Nie, Q. Zhang, Q. Ma, *Analytical Chemistry* **2019**, *91*, 6250-6258.

[30] H. Peng, M. Jian, H. Deng, W. Wang, Z. Huang, K. Huang, A. Liu, W. Chen, *ACS Appl. Mater. Interfaces* **2017**, *9*, 14929-14934.

[31] A. Han, Y. Yang, Q. Zhang, Q. Tu, G. Fang, J. Liu, S. Wang, R. Li, *Journal of Electroanalytical Chemistry* **2017**, *795*, 116-122.